Journal of Alloys and Compounds 488 (2009) 254–259

Contents lists available at ScienceDirect

Journal of Alloys and Compounds

journal homepage: www.elsevier.com/locate/jallcom

# Magnetic and electrical properties of $Bi_{0.8}Ca_{0.2}Fe_{1-x}Mn_xO_3$ ($0 \le x \le 0.5$)

L.H. Yin [a], Y.P. Sun [a,*], F.H. Zhang [b], W.B. Wu [b], X. Luo [a], X.B. Zhu [a], Z.R. Yang [a], J.M. Dai [a], W.H. Song [a,*], R.L. Zhang [c]

[a] Key Laboratory of Materials Physics, Institute of Solid State Physics, and High Magnetic Field Laboratory, Chinese Academy of Sciences, Hefei 230031, People's Republic of China
[b] Hefei National Laboratory for Physics Sciences at the Microscale, University of Science and Technology of China, Hefei 230026, People's Republic of China
[c] Ningbo Institute of Material Technology and Engineering, Chinese Academy of Sciences, Ningbo 315040, PR China

ARTICLE INFO

*Article history:*
Received 6 April 2009
Received in revised form 20 August 2009
Accepted 21 August 2009
Available online 29 August 2009

*PACS:*
72.15.Eb
75.50.Cc
65.90.+i

*Keywords:*
Bismuth ferrite
Multiferroics

ABSTRACT

Mn-substituted $Bi_{0.8}Ca_{0.2}FeO_3$ ceramics $Bi_{0.8}Ca_{0.2}Fe_{1-x}Mn_xO_3$ ($0 \le x \le 0.5$) were synthesized by a solid-state reaction method. Powder X-ray diffraction investigations performed at room temperature show that the crystal structure is rhombohedral for $x \le 0.1$ and orthorhombic for $0.2 \le x \le 0.5$. Compared to the undoped $Bi_{0.8}Ca_{0.2}FeO_3$ compound, enhanced magnetization and electric polarization were observed in the samples with $x \le 0.1$. A further increase in the magnetization with increasing $x$ took place in the samples with $0.2 \le x \le 0.5$. All the Mn-substituted samples studied are basically antiferromagnetic accompanied by the appearance of weak ferromagnetism, which is similar to the $BiFeO_3$ compound. The conductivity of the samples with $x \ge 0.3$, measured between 140 and 380 K, is of the semiconducting type.


## 1. Introduction

Much attention has been paid to the multiferroic materials that exhibit both magnetic and ferroelectric (FE) properties recently [1–3]. A lot of interesting phenomena can be produced by the coupling between the magnetic and FE degrees of freedom in multiferroics, such as the magnetoelectric (ME) effect, in which the electric polarization can be tuned by applied magnetic field and vice versa [1–3]. Because of these new spectacular properties, multiferroic materials can have many interesting and promising potential applications. However, there are only a few materials exhibiting both ferromagnetic (FM) and FE behaviors. For $ABO_3$ perovskite compounds, theoretical studies have shown that the mechanisms for magnetism and ferroelectricity are usually mutually exclusive in the same material [4] and empirically there are indeed few multiferroic materials. Among the few multiferroics, Bi-based perovskites are one important class of multiferroics, in which the FM is due to the B-site transitional metal ions and the FE is due to the A-site Bi ions [5]. $BiFeO_3$ is one of the few well-known multiferroics that exhibits both FE order ($T_C$ = 1100 K) and G-type antiferromagnetic (AFM) order ($T_N$ = 643 K) simultaneously. It possesses a rhombohedrally distorted perovskite structure with space group *R3c* at room temperature (RT) [6]. Due to the canting of the AFM sublattices, $BiFeO_3$ exhibits weak FM even at RT. Meanwhile, a nearly sinusoidal spin structure along $[1\,1\,0]_h$ leads to the cancellation of the macroscopic magnetization and the prohibition for observing the linear ME effect [7]. This spiral spin structure can be suppressed or even destroyed by chemical substitutions [8,9]. Recently, enhancement of magnetization has been reported in $Bi_{1-x}A_xFeO_3$ ($A = Ba^{2+}$, $La^{3+}$, $Ca^{2+}$, $Sr^{2+}$) materials [9–12] and it is thought that the substitution could suppress the incommensurate spin configuration and cause the enhancement of the magnetization. However, the B-site ion doping is a more direct and effective way to affect the magnetic properties in $ABO_3$ type perovskites while keeping the FE properties similar to the parent compounds [13,14], and enhanced magnetization is indeed observed in the Mn-doped $BiFeO_3$ compound [15,16]. In the present work, we report the effect of Mn-doping at Fe-site on the crystal structure, magnetic and electrical properties of multiferroic $Bi_{0.8}Ca_{0.2}FeO_3$.

## 2. Experimental

Polycrystalline $Bi_{0.8}Ca_{0.2}Fe_{1-x}Mn_xO_3$ ($x$ = 0, 0.05, 0.1, 0.2, 0.3, 0.4 and 0.5) samples were prepared by a conventional solid-state reaction method from high purity $Bi_2O_3$, $Fe_2O_3$, $MnO_2$ and $CaCO_3$. The stoichiometric powders were mixed thoroughly, placed into $Al_2O_3$ crucibles and then fired in air at 750 °C for 24 h. The resultant powders were ground, pressed into small pellets and sintered at 850 °C for 24 h and finally at 900 °C for another 24 h with intermediate grinding.

The RT X-ray diffraction (XRD) measurements were taken by Philips X'pert PRO X-ray diffractometer with Cu $K_\alpha$ radiation. The structural parameters were obtained

* Corresponding authors. Tel.: +86 551 5592757; fax: +86 551 5591434.
*E-mail addresses:* ypsun@issp.ac.cn (Y.P. Sun), whsong@issp.ac.cn (W.H. Song).

0925-8388/$ – see front matter © 2009 Elsevier B.V. All rights reserved.
doi:10.1016/j.jallcom.2009.08.099

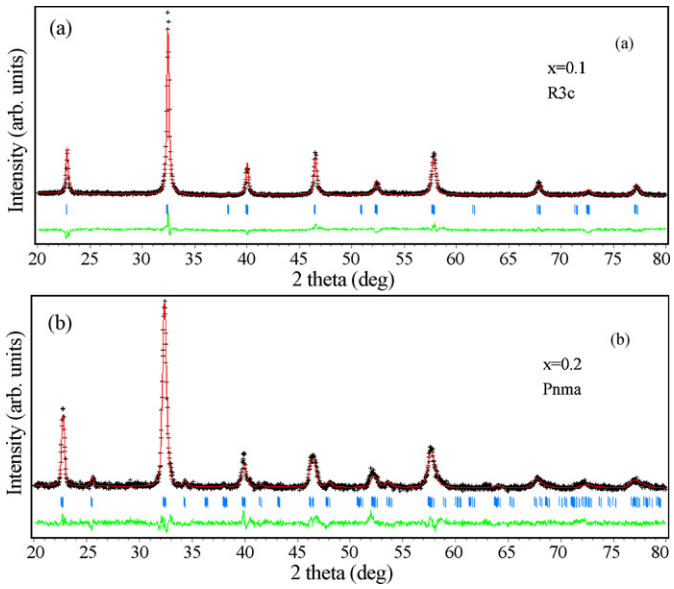


**Fig. 1.** Powder XRD patterns of the samples $Bi_{0.8}Ca_{0.2}Fe_{1-x}Mn_xO_3$ with $x = 0.1$ (a) and $x = 0.2$ (b) at RT, respectively. Crosses indicate the experimental data and the calculated data is the continuous line overlapping them. The lowest curve shows the difference between experimental and calculated patterns. The vertical bars indicate the expected reflection positions.

by fitting the experimental data of XRD using the standard Rietveld technique. The resistance as a function of temperature was measured by the standard four-probe method from 140 to 380 K. Differential thermal analysis (DTA) was used to determine the FE phase transition temperature ($T_C$). Dielectric measurements were performed at 25 °C using an LCR meter in the frequency range 100 Hz to 1 MHz. RT FE hysteresis loops were measured by using TF Analyzer 2000 (aixACCT) at a frequency of 1 kHz. The magnetic measurements were carried out with a quantum design superconducting quantum interference device (SQUID) MPMS system.

## 3. Results and discussion

The RT XRD results show that all $Bi_{0.8}Ca_{0.2}Fe_{1-x}Mn_xO_3$ ($0 \le x \le 0.5$) samples are single phase with no detectable secondary phases. The XRD patterns of the samples with $0 \le x \le 0.1$ can be indexed by a rhombohedral lattice with space group *R*3*c*, which is the same with the compound $BiFeO_3$. While the XRD patterns of the samples with $0.2 \le x \le 0.5$ can be indexed by an orthorhombic lattice with space group *Pnma*. The structural parameters are refined by the standard Rietveld technique [17] and the fitting between the experimental spectra and the calculated values is relatively good based on the consideration of relatively lower $R_p$ (<10%) values. Fig. 1 shows experimental and calculated XRD patterns for the two representative samples with $x = 0.1$ and 0.2, respectively. The structural parameters obtained are plotted versus $x$ in Fig. 2. As we can see, for samples with $0 \le x \le 0.1$, with the increase in Mn content there is a decrease in both $a$ and $c$ parameters of the unit cell. It results in unit cell volume contraction. This is expected since ionic radius of $Mn^{4+}$ (0.53 Å) is slightly smaller than that of $Fe^{3+}$ (0.645 Å). While for samples with $0.2 \le x \le 0.5$, the unit cell volume also contracts with increasing Mn content $x$. This is contrary to the anticipation that there will be only a small structural impact if any, if we expect the ionic ratio to be $Bi_{0.8}Ca_{0.2}Fe^{3+}{}_{0.8-y}Mn^{4+}{}_{0.2}Mn^{3+}{}_yO_3$ ($0 \le y \le 0.3$) with practically identical ionic radius for $Mn^{3+}$ and $Fe^{3+}$ (0.645 Å). This anomaly has also been reported in $Bi_{0.5}Ca_{0.5}Fe_xMn_{1-x}O_3$ ($0 \le x \le 0.6$) systems recently [18].

It is reported that $Bi_{0.9}La_{0.1}Fe_{1-x}Mn_xO_3$ ($0 \le x \le 0.5$) compounds possess a rhombohedrally distorted structure and keep FE characteristics similar to $BiFeO_3$ in the whole doping range [15]. Recently $Bi_{1-x}Sr_xFe_{0.8}Mn_{0.2}O_3$ ($0 < x \le 0.2$) ceramics have also been reported

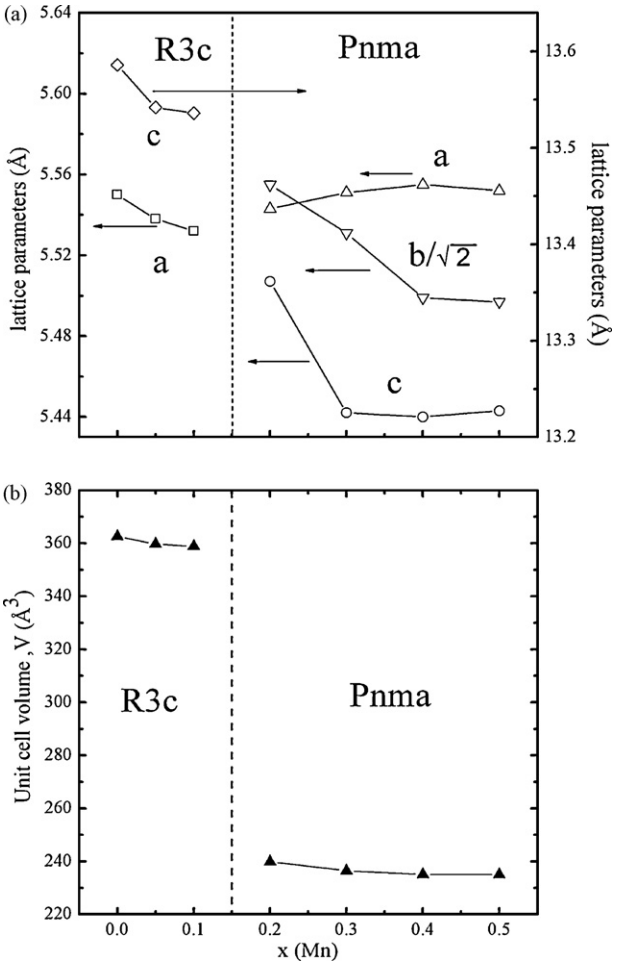


**Fig. 2.** (a) Mn substitution dependence of the lattice parameters, $a$, $\sqrt{b}$, $c$ and (b) unit cell volume, $v$.

to be multiferroic [19]. Similarly, we can also expect that our samples with $x \le 0.1$, which possess noncentrosymmetric rhombohedral structure, keep the FE properties similar to the parent compound $Bi_{0.8}Ca_{0.2}FeO_3$ with the same structure [11]. In order to verify this hypothesis, a DTA study was carried out on the representative sample with $x = 0.1$, which is shown in Fig. 3. A peak in the DTA curve can be observed at around 854 °C, which might be due to the FE transition. Previous reports on the $BiFeO_3$ [20], $Bi_{0.9}La_{0.1}Fe_{1-x}Mn_xO_3$ [15] and $Bi_{1-x}Sr_xFe_{0.8}Mn_{0.2}O_3$ [19] have

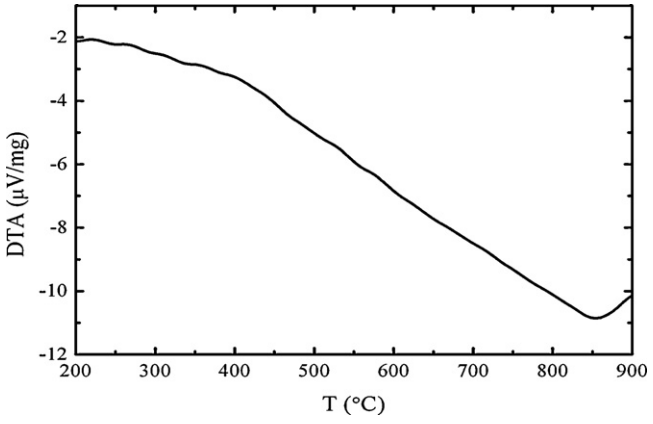


**Fig. 3.** The DTA curve obtained for the $Bi_{0.8}Ca_{0.2}Fe_{0.9}Mn_{0.1}O_3$ sample indicating presence of ferroelectric transition ($T_C$) at ~854 °C.

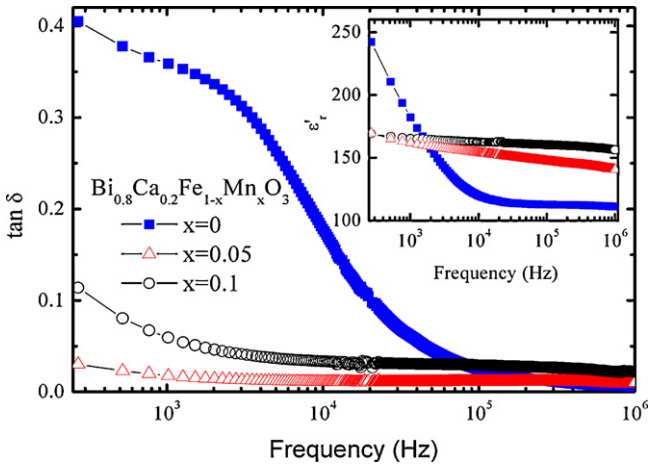


**Fig. 4.** The loss tangent (tan $\delta$) and relative dielectric constant ($\varepsilon_r'$) (shown in the inset) for the samples $Bi_{0.8}Ca_{0.2}Fe_{1-x}Mn_xO_3$ with $x \leq 0.1$ in the frequency range of 100 Hz to 1 MHz at 25 °C.

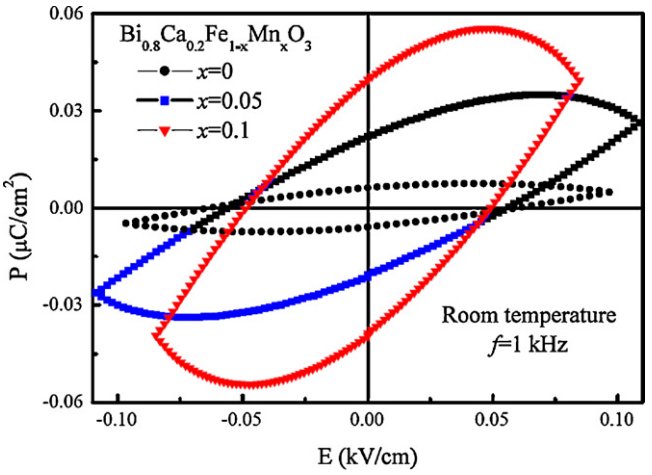


**Fig. 5.** RT polarization–electric field hysteresis loops $P(E)$ measured at a frequency of 1 kHz for the samples with $x \leq 0.1$.

attributed the peak observed in DTA in the vicinity of 830 °C to FE phase transition. The slight increase in $T_C$ of our sample might result from the change of lattice distortion due to the $Ca^{2+}$ and $Mn^{4+}$ substitution. However, the samples with $x \geq 0.2$ possess centrosymmetric orthorhombic structure, implying the absence of FE in them at least at RT. There may exist some very interesting physical phenomena in the vicinity of the critical structural phase transition point, which is worth studying further.

Fig. 4 and the inset show the variation of loss tangent (tan $\delta$) and relative dielectric constant ($\varepsilon_r'$) with frequency for the samples $Bi_{0.8}Ca_{0.2}Fe_{1-x}Mn_xO_3$ with $x \leq 0.1$ at 25 °C. Compared to the parent compound $Bi_{0.8}Ca_{0.2}FeO_3$, the Mn-substituted samples show substantial decrease in both $\varepsilon_r'$ and tan $\delta$ at low frequencies, which indicates reduced conductivity in the doped samples [21]. Their dielectric traits, such as low dielectric loss tangent (tan $\delta$) of 0.030 at 270 Hz for the sample with $x = 0.05$ and the weak dependence of $\varepsilon_r'$ on frequency, indicate that dipoles with small effective masses (e.g., electrons and ferroelectric domain walls) mainly contribute to $\varepsilon_r'$ instead of charged defects with large effective masses (e.g., oxygen vacancies). The improved dielectric properties at low frequencies for the Mn-substituted samples can also be explained in the following way: Mn substitution in the compound $Bi_{0.8}Ca_{0.2}FeO_3$ decreases the oxygen vacancies through the formation of $Mn^{4+}$ and thus decreases the low-frequency $\varepsilon_r'$ and tan $\delta$. Note that it has been reported that the heterovalent $Pb^{2+}$ substitution in $Bi_{0.8}Pb_{0.2}FeO_y$ has led to the formation of oxygen vacancies [22].

The RT polarization–electric field ($P$–$E$) measurements at a frequency of 1 kHz for the samples with $x \leq 0.1$ reveal both a FE and a leaky behavior of the samples, which are shown in Fig. 5. At the maximum applied electric field, the remnant polarizations ($P_r$) are 0.006, 0.022 and 0.039 μC/cm$^2$ for $x = 0$, 0.05 and 0.1, respectively. Clearly, the remnant polarization increases with increasing Mn substitution. However, fully saturated hysteresis loops could not be obtained due to the leaky nature of the samples.

The temperature dependences of magnetization between 5 and 380 K in the field cooling (FC) measuring mode at $H = 100$ Oe for the samples $Bi_{0.8}Ca_{0.2}Fe_{1-x}Mn_xO_3$ with $x \leq 0.1$ are shown in Fig. 6(a). We can see that, the magnetization increases with the increase of the Mn content in the sample. The magnetic hysteresis loops are shown in Fig. 6(b). It can be clearly seen that the predominant character of the response is linear in the field but a weak FM response also exists, which is especially obvious for the sample with $x = 0.1$ (the remnant magnetization $M_r$ and coercivity $H_c$ for it are 0.06 emu/g and 5.5 kOe, respectively). The zero field cooled (ZFC) and FC magnetization curves at 100 Oe for the sample with $x = 0.1$ are presented in Fig. 7. A great discrepancy between ZFC and FC curves and the cusp in ZFC at low temperature can be clearly seen for this sample. Such behavior has already been observed for lots of manganites in the same temperature range. Different factors, such as, magnetic disorder, magnetic frustration and the existence of small magnetic particles, can result in this behavior. In our case, the possible competing $Fe^{3+}$–O–$Mn^{4+}$ FM and $Fe^{3+}$–O–$Fe^{3+}$ or $Mn^{4+}$–O–$Mn^{4+}$ AFM interactions, or the mechanism similar to what leads to the low temperature spin glass behavior in the compound $BiFeO_3$ [23], might cause this behavior observed in the samples

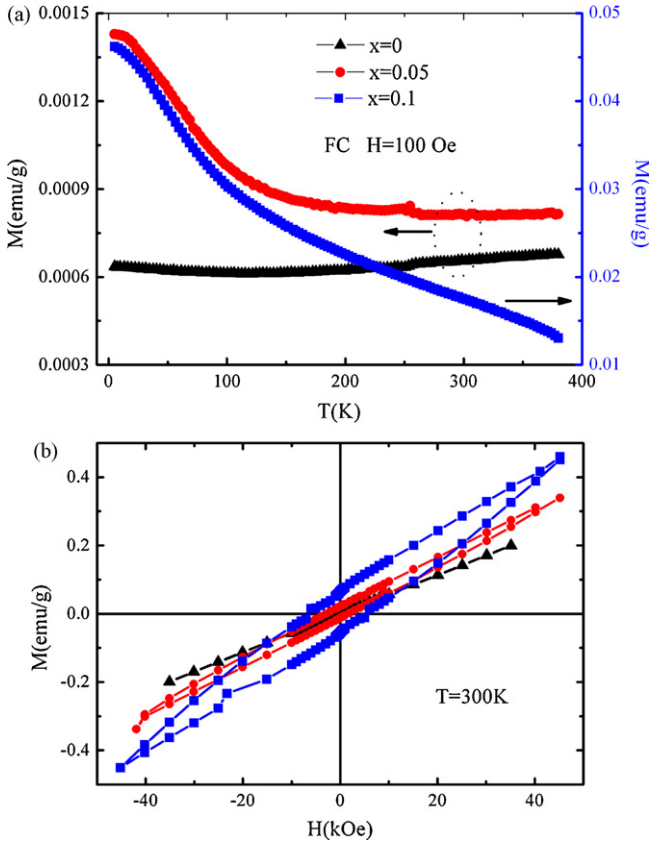


**Fig. 6.** (a) The temperature dependence of magnetization for the samples $Bi_{0.8}Ca_{0.2}Fe_{1-x}Mn_xO_3$ with $x \leq 0.1$ between 5 and 180 K at 100 Oe. (b) Field dependence of magnetization for the samples with $x \leq 0.1$ at RT.

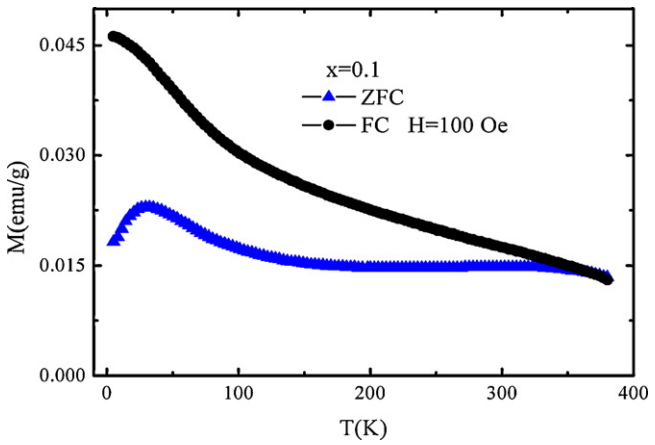


**Fig. 7.** Magnetization versus temperature ($M$–$T$) curves at 100 Oe for the sample with $x = 0.1$.

with $x \leq 0.1$. However, more extended and detailed study (such as, magnetic field effects on properties) might throw some light on this behavior. These results support the fact that the samples with $x \leq 0.1$ are basically AFM but have a weak FM. The origin of the weak FM may be due to the small spin canting and the suppression of the spiral spin structure due to Mn substitution [24], or the possible $Fe^{3+}$–O–$Mn^{4+}$ FM interactions.

The temperature dependence of magnetization in different fields for the sample with $x = 0.2$ are shown in Fig. 8. There are two clear maxima in the low field ZFC curve at $T_{max1} = 23$ K and $T_{max2} = 45$ K, and the FC curve deviates significantly from the ZFC one well above $T_{max2}$. But this effect is smeared in higher fields, which can be seen in the inset of Fig. 8. The deviation of FC curves from the ZFC ones can be considered as an indication that a great magnetic inhomogeneity exists in the sample and the transition at $T_{max2}$ is of magnetic nature. This transition is not of pure AFM type. Either some FM phase coexists with the main AFM one, or the AFM is accompanied by a so-called weak FM of Dzyaloshinskii–Moriya type. The latter possibility seems to be more reasonable, because the peak disappears in higher fields and similar behavior has also been observed in the $Bi_{0.5}Ca_{0.5}Fe_xMn_{1-x}O_3$ ($0 \leq x \leq 0.6$) and other systems [18,25]. This suggestion is also supported by the fact that almost in all of our lightly Mn-doped samples a significant divergence between the FC and ZFC curves was observed, especially in the low temperature region. This fact as well as a large coercive field evidences a significant magnetic anisotropy as it will be shown later.

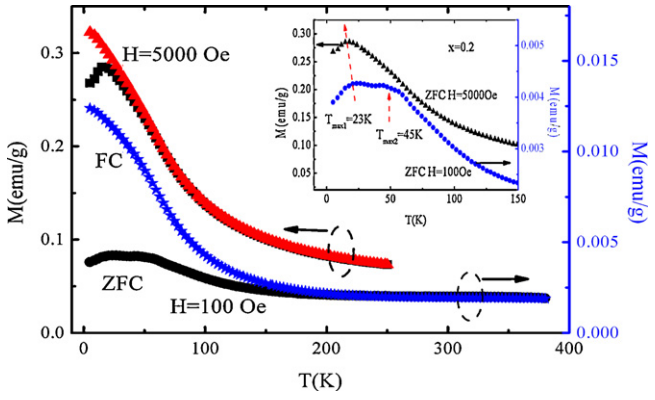


**Fig. 8.** Magnetization as a function of temperature in ZFC and FC processes with applied fields 100 and 5000 Oe for the sample with $x = 0.2$. Inset, an enlarged part around the local magnetization maximum in the ZFC curves with different applied fields.

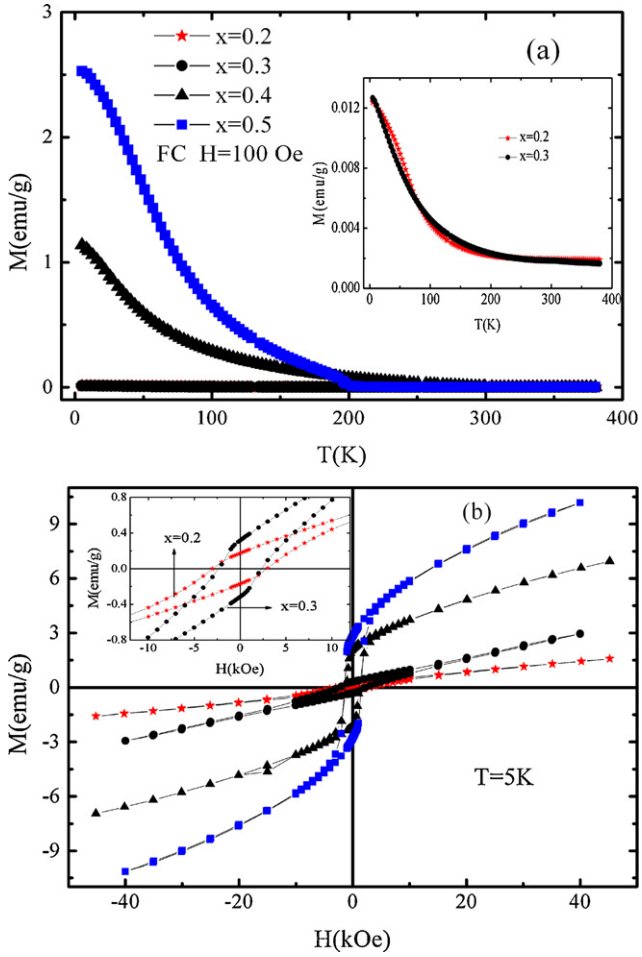


**Fig. 9.** (a) The $M$–$T$ curves (FC) at $H = 100$ Oe obtained for the samples with $0.2 \leq x \leq 0.5$. Inset, enlarged $M$–$T$ curves for the samples with $x = 0.2$, 0.3. (b) $M$–$H$ curves for the samples with $0.2 \leq x \leq 0.5$ at 5 K. Inset, a more close sight for the samples with $x = 0.2$, 0.3.

The cusp at $T_{max1}$ and the greater discrepancy between ZFC and FC curves below this temperature for the sample with $x = 0.2$ are very similar to those observed for the samples with $x \leq 0.1$ as discussed above. In fact, both the splitting temperature and the cusp shifting to lower temperature under a higher magnetic field of 5000 Oe were really observed here, as can be seen in the inset of Fig. 8.

Fig. 9(a) shows the FC curves of the samples with $0.2 \leq x \leq 0.5$. There is a great increase in magnetization with increasing $x$. This increase can also be obviously seen in the magnetic hysteresis loops at 5 K as shown in Fig. 9(b). Another feature was observed in the samples with $x \geq 0.3$. There are two kinks in both ZFC and FC curves for all the samples, especially obvious for the sample with $x = 0.5$. The higher temperature kink shifts toward lower temperature with increasing $x$. The temperature, at which the ZFC curve starts to deviate from the FC one, decreases with increasing Mn content. This indicates that the samples become more homogeneous with higher Mn substitution. In order to further study the magnetic properties, the $M$–$T$ curves in different applied fields for the sample with $x = 0.5$ are plotted in Fig. 10. Two magnetic transitions can be clearly seen in the low field $M$–$T$ curves, and the higher transition temperature $T_C$ is around 196 K. The kink at this temperature becomes less obvious in a higher field of 10,000 Oe. This behavior is rather similar to that of the sample with $x = 0.2$ as discussed above. We remember that one of the characteristics of the canted antiferromagnetic (CAF) structure is that the magnetic interactions in the sample are pre-

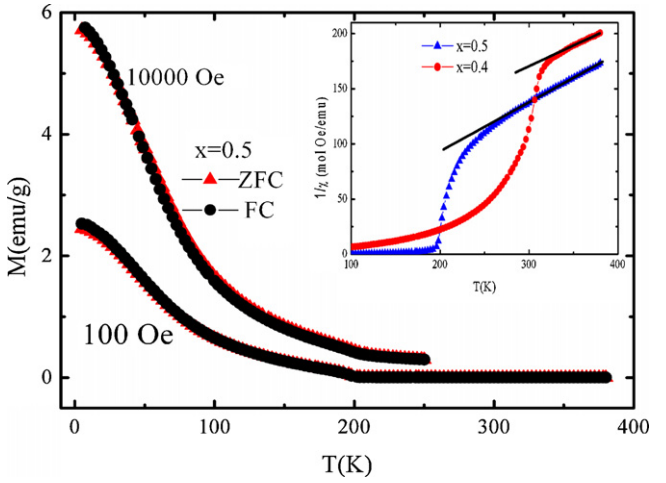


**Fig. 10.** The $M$–$T$ curves for the sample with $x = 0.5$ at $H = 100$ Oe and 10,000 Oe. Inset, the inverse susceptibility as a function of temperature in the ZFC processes for the samples with $x = 0.4$, 0.5. The solid lines stand for Curie–Weiss fitting.

dominantly AFM, but below the transition temperature $T_C$ a small spontaneous moment develops, resulting in a magnetic state that can be described as a weak FM state [26,27]. Keeping this in mind and considering the fact that the sign of the Curie temperature is negative for our samples deduced from the high temperature Curie–Weiss fitting as it will be discussed later, we can consider the magnetic behavior below $T_C$ (196 K) as the canted AFM state, which is analogous to those observed for the samples with $x \leq 0.2$.

For the samples with $x = 0.4$ and 0.5, we fitted the experimental data in high temperature region according to the Curie–Weiss law, $\chi = C/(T - \theta_P)$. The temperature dependence of the inverse magnetic susceptibility, $1/\chi$, and the fitting curves are shown in the inset of Fig. 10. The effective magnetic moment $\mu_{\text{eff}}$ values and paramagnetic Curie–Weiss temperatures $\theta_P$ of the two samples with $x = 0.4$ and 0.5 deduced from experiments are 4.531 $\mu_B$, −134 K and 4.247 $\mu_B$, −10 K, respectively. The negative signs of $\theta_P$ confirm the AFM behavior of the samples. Both of the effective magnetic moment $\mu_{\text{eff}}$ values obtained from experiment for the two samples are smaller than the calculated ones by assuming the stoichiometry of the compounds with the ionic ratio $Bi_{0.8}Ca_{0.2}Fe^{3+}{}_{0.6}Mn^{4+}{}_{0.2}Mn^{3+}{}_{0.2}O_3$ and $Bi_{0.8}Ca_{0.2}Fe^{3+}{}_{0.5}Mn^{4+}{}_{0.2}Mn^{3+}{}_{0.3}O_3$ (i.e., 5.294 and 5.254 $\mu_B$, respectively). We can explain this fact if we assume that the AFM interaction of $Fe^{3+}$ ions with surrounding ions is so strong that even at relatively high temperature the magnetic moments of some $Fe^{3+}$ ions have no contribution (similar to the formation of spin-singlet states). In this context, we note that $BiFeO_3$ and $Bi_{0.8}Ca_{0.2}FeO_3$ are AFM with the Néel temperature far above RT.

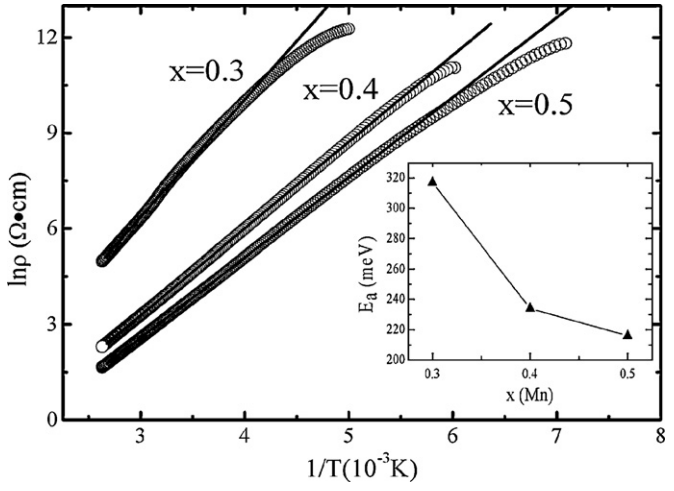


**Fig. 11.** The plot of ln $\rho$ against $T^{-1}$ for the $Bi_{0.8}Ca_{0.2}Fe_{1-x}Mn_xO_3$ compounds with $x = 0.3$, 0.4, 0.5. The solid lines stand for TAC fitting. The inset shows the variation of activation energy $E_a$.

The samples with $x = 0.3$, 0.4, 0.5 exhibit a semiconductor-type electrical resistivity as shown in Fig. 11. The absolute value of the resistivity decreases with increasing Mn content, which could be attributed to the increasing of $Mn^{3+}$ ions with weaker mobile $e_g$ electrons. The high temperature $\rho(T)$ data can be fitted by the thermally activated conduction (TAC) law, $\rho(T) = \rho_0 \exp(E_a/k_B T)$, where $E_a$ is the activation energy. As we can see in the inset of Fig. 10, the value of $E_a$ gradually decreases from 317 meV ($x = 0.3$) to 216 meV ($x = 0.5$) with increasing Mn content.

## 4. Conclusions

In conclusion, we have studied the effect of Mn substitution on the crystal structure, magnetic and electrical properties of the multiferroic $Bi_{0.8}Ca_{0.2}FeO_3$. Single phase $Bi_{0.8}Ca_{0.2}Fe_{1-x}Mn_xO_3$ ($0 \leq x \leq 0.5$) samples have been prepared through solid state reaction. A structural phase transition from rhombohedral to orthorhombic is observed near $x = 0.2$. For the samples with $x \leq 0.1$, enhanced magnetization and electric polarization and substantially decreased low-frequency dielectric loss tangent at RT were achieved compared to the parent compound $Bi_{0.8}Ca_{0.2}FeO_3$. The samples $Bi_{0.8}Ca_{0.2}Fe_{1-x}Mn_xO_3$ ($0.2 \leq x \leq 0.5$) show a greater increase in magnetization with increasing $x$. The presence of a small spontaneous magnetization in all the samples can be explained by AFM accompanied by a weak FM component. The substitution of Mn for Fe in the B-site has resulted in the enhanced FM by the possible $Fe^{3+}$–O–$Mn^{4+}$ FM interactions, or the suppression of the incommensurate spin configuration and causing a small spin canting. The conductivity of the compounds with $0.3 \leq x \leq 0.5$ is of semiconducting type. These results may be helpful for further study on the multiferroic properties of $BiFeO_3$-based solid solutions.

## Acknowledgments

This work was supported by the National Key Basic Research under Contract No. 2007CB925001, the National Science Foundation (NSF) of China under Contract Nos. 50672099, 10874166, 10874051, Anhui Provincial NSF Grant No. 070416233, and Zhejiang Provincial NSF Grant No. Y606831.

## References

[1] S.-W. Cheong, M. Mostovoy, Nat. Mater. 6 (2007) 13.
[2] W. Eerenstein, N.D. Mathur, J.F. Scott, Nature (London) 442 (2006) 759.
[3] H. Schmid, J. Phys.: Condens. Matter 20 (2008) 434201.
[4] N.A. Hill, J. Phys. Chem. B 104 (2000) 6694.
[5] R. Seshadri, N.A. Hill, Chem. Mater. 13 (2001) 1892.
[6] A.J. Jacobson, B.E.F. Fender, J. Phys. C 8 (1975) 844.
[7] C. Ederer, N.A. Spaldin, Phys. Rev. B 71 (2005), 060401 (R).
[8] A. Singh, V. Pandey, R.K. Kotnala, D. Pandey, Phys. Rev. Lett. 101 (2008) 247602.
[9] V.A. Khomchenko, V.V. Shvartsman, P. Borisov, W. Kleemann, D.A. Kiselev, I.K. Bdikin, J.M. Vieira, A.L. Kholkin, J. Phys. D: Appl. Phys. 42 (2009) 045418.
[10] S.-T. Zhang, Y. Zhang, M.-H. Lu, C.-L. Du, Y.-F. Chen, Z.-G. Liu, Y.-Y. Zhu, N.-B. Ming, X.Q. Pan, Appl. Phys. Lett. 88 (2006) 162901.
[11] V.A. Khomchenko, D.A. Kiselev, J.M. Vieira, A.L. Kholkin, M.A. Sá, Y.G. Pogorelov, Appl. Phys. Lett. 90 (2007) 242901.
[12] L.Y. Wang, D.H. Wang, H.B. Huang, Z.D. Han, Q.Q. Cao, B.X. Gu, Y.W. Du, J. Alloys Compd. 469 (2009) 1.
[13] J.-B. Li, G.H. Rao, J.K. Liang, Y.H. Liu, J. Luo, J.R. Chen, Appl. Phys. Lett. 90 (2007) 162513.
[14] N. Riad, H. Catalin, P. Alain, N. Francois, V. Teodor, C. Louis-Philippe, M. David, Appl. Phys. Lett. 89 (2006) 102902.
[15] V.R. Palkar, Darshan C. Kundaliya, S.K. Malik, J. Appl. Phys. 93 (2003) 4337.
[16] A.K. Kundu, R. Ranjith, B. Kundys, N. Nguyen, V. Caignaert, V. Pralong, W. Prellier, B. Raveau, Appl. Phys. Lett. 93 (2008) 052906.

[17] L.B. Mccusker, R.B. Von Dreele, D.E. Cox, D. Louër, P. Scandi, J. Appl. Cryst. 32 (1999) 36.
[18] D. Tzankov, D. Kovacheva, K. Krezhov, R. Puzniak, A. Wiśniewski, E. Sváb, M. Mikhov, J. Phys.: Condens. Matter 17 (2005) 4319.
[19] Jie Wei, Desheng Xue, Electrochem. Solid-State Lett. 10 (2007) G85.
[20] W. Kaczmarek, Z. Pajak, M. Polomska, Solid State Commun. 17 (1975) 807.
[21] S.R. Das, P. Bhattacharya, R.N.P. Choudhary, R.S. Katiyar, J. Appl. Phys. 99 (2006) 066107.
[22] V.A. Khomchenko, D. AKiselev, J.M. Vieira, R.M. Rubinger, N.A. Sobolev, M. Kopcewicz, V.V. Shvartsman, P. Borisov, A. WKleemann, L. Kholkin, J. Phys.: Condens. Matter 20 (2008) 155207.
[23] Manoj K. Singh, W. Prellier, M.P. Singh, Ram S. Katiyar, J.F. Scott, Phys. Rev. B 77 (2008) 144403.
[24] I. Sosnowskal, W. Schäfer, W. Kockelmann, K.H. Andersen, I.O. Troyanchuk, Appl. Phys. A 74 (2002) S1040.
[25] A.K. Azad, S. Ivanov, S.-G. Eriksson, H. Rundlöf, J. Eriksen, R. Mathieu, P. Svedlindh, J. Magn. Magn. Mater. 237 (2001) 124.
[26] G. Amow, J.E. Greedan, C. Ritter, J. Solid State Chem. 141 (1998) 262.
[27] A.K. Azad, S.A. Ivanov, S.-G. Eriksson, J. Eriksen, H. Rundlöf, R. Mathieu, P. Svedlindh, Mater. Res. Bull. 36 (2001) 2215.